ELSEVIER

Earth and Planetary Science Letters 182 (2000) 157–169

EPSL

www.elsevier.com/locate/epsl

A thermo-mechanical model of horizontal subduction below an overriding plate

Jeroen van Hunen *, Arie P. van den Berg, Nico J. Vlaar

Department of Theoretical Geophysics, Institute of Earth Sciences, Utrecht University, 3508 TA Utrecht, The Netherlands

Received 6 January 2000; received in revised form 7 August 2000; accepted 9 August 2000

Abstract

Subduction of young oceanic lithosphere cannot be explained by the gravitational driving mechanisms of slab pull and ridge push. This deficiency of driving forces can be overcome by obduction of an actively overriding plate, which forces the young plate either to subduct or to collide. This mechanism leads to shallow flattening of the slab as observed today under parts of the west coast of North and South America. Here this process is examined by means of numerical modeling. The convergence velocity between oceanic and continental lithospheric plates is computed from the modeling results, and the ratio of the subduction velocity over the overriding velocity is used as a diagnostic of the efficiency of the ongoing subduction process. We have investigated several factors influencing the mechanical resistance working against the subduction process. In particular, we have studied the effect of a preexisting lithospheric fault with a depth dependent shear resistance, partly decoupling the oceanic lithosphere from the overriding continent. We also investigated the lubricating effect of a 7 km thick basaltic crustal layer on the efficiency of the subduction process and found a log–linear relation between convergence rate and viscosity prefactor characterizing the strength of the oceanic crust, for a range of parameter values including values for basaltic rocks, derived from empirical data. A strong mantle fixes the subducting slab while being overridden and prevents the slab from further subduction in a Benioff style. Viscous heating lowers the coupling strength of the crustal interface between the converging plates with about half an order of magnitude and therefore contributes significantly to the subduction process. Finally, when varying the overriding velocity from 2.5 to 10 cm yr^{-1}, we found a non-linear increase of the subduction velocity due to the presence of non-linear mantle rheology. These results indicate that active obduction of oceanic lithosphere by an overriding continental lithosphere is a viable mechanism for shallow flat subduction over a wide range of model parameters.

Keywords: subduction; rheology; viscosity; plates; mantle

1. Introduction

Gravitational instability forces such as slab pull and ridge push mainly drive Benioff type of subduction, while the most important resistance comes from internal friction and friction or drag from the overriding plate and mantle below. The dominance of slab pull and ridge push over the resisting forces makes subduction an active process: the net driving force is internally created. For young oceanic plates, however, resisting

* Corresponding author. Tel.: +31-30-253 5141; Fax: +31-30-253-3486; E-mail: hunen@geo.uu.nl

0012-821X/00/$ – see front matter
PII: S0012-821X(00)00240-5

forces would dominate in this setup, since oceanic plates younger than about 30 Ma are gravitationally stable due to the buoyant lithosphere. In this case, other driving forces are necessary for subduction to occur. Vlaar [1] proposed the lithospheric doubling scenario as a possible mechanism: in this scenario a continent overrides a young oceanic plate (obduction) and this plate subducts rather passively along with the mantle underneath. Reconstructions of absolute plate motion show an overriding velocity at subduction zones along the western Americas in the past and present [2–5]. Lithospheric doubling would result in shallow flattening of the subducted slab and could therefore be an explanation for the flat slab segments which have been observed using various geological and geophysical methods. A similar effect could be expected from an eastward moving mantle as suggested in [5]. Vlaar and Wortel [6] investigated dip angles of subducting plates defined by means of earthquake hypocenters. They suggested a correlation might be present between the lithospheric age and the dip angle of the subducting slab. Cross and Pilger [7] suggest a correlation between the dip angle to be dependent on absolute overriding plate motion, convergence rate, slab age and the subduction of aseismic ridges. Flat subduction probably occurred around 65 Ma ago below the western USA and may have caused the Laramide orogeny and related tectonic features [8–10]. This has been concluded from seismic data, heat flow measurements, migrating patterns of magmatism, tectonic reconstructions and tomographic images. Present-day horizontal subduction occurs at the west coast of Mexico and central Chile [6,11–13].

Other mechanisms for flat lying subduction have previously been proposed. The 670 km discontinuity phase change can easily result in flat lying slabs in case of sufficient roll-back [14–16]. However, this occurs in the transition zone and not at shallow depth, directly below the overriding plate. Furthermore, the trench roll-back is a result of the pulling force which is generated by an old and heavy slab and not by young and gravitationally stable slabs. Buoyant plateaus may give an explanation for shallow flattening of the subducting plates [13], but do not form a driving mechanism for this type of subduction. With adherence to the overriding plate by a non-hydrostatic pressure force [17] or a slab suction force [18,19], a deflection of the subducting slab towards the horizontal can be explained. These models, however, do not propose a driving force for flat subduction, but merely a mechanism to flatten an already subducting plate.

Plate tectonics are characterized by strain concentration within the plate margins. Large strains are accommodated by fault systems between the converging plates. The importance of such faults in the dynamics of the subduction process has been shown in [14,20]. Localized ductile deformation is observed in models using highly non-linear stress weakening rheologies [20–22]. Other mechanisms are provided by compositionally defined lubricants, such as a hydrated oceanic crust [23], or by viscous heating [24,25]. Here, we investigate the relative importance of faults, crustal strength and mantle strength in the process of lithospheric doubling by means of numerical modeling. First, we present the numerical model, including the implementation of a lithospheric fault and tracking of compositional differences. Next, we examine the influence on the subduction dynamics of various model parameters systematically. Finally, we discuss the applications of the results for the Earth.

2. Model description

2.1. Governing equations

We assume an incompressible medium with infinite Prandtl number and we apply the extended Boussinesq approximation [26]. We use the same non-dimensionalization scheme as in [27]. The non-dimensional continuity and momentum equation are respectively:

$$\partial_j u_j = 0 \tag{1}$$

$$\partial_j(\eta e_{ij}) - \partial_i \Delta p = (RaT + RcC)\delta_{iz} \tag{2}$$

in which both thermal and compositional buoyancy are accounted for in the right hand side of

Eq. 2. Symbols used are defined in Table 1. A compositional (crust–mantle) layering for the subducting oceanic lithosphere is defined through a bi-valued composition distribution $C(\boldsymbol{x})$ which is advected with the flow. The non-diffusive transport equation for the composition:

$$\frac{\partial C}{\partial t} + u_j \partial_j C = 0 \tag{3}$$

is solved using a Lagrangian particle tracer method (see Section 3). Both buoyancy and effective viscosity are defined to be dependent on the composition. This way, we have used different rheological flow laws for the basaltic oceanic crust and underlying mantle. Conservation of energy is described by the non-dimensional heat equation:

$$\frac{\partial T}{\partial t} + u_j \partial_j T - Di(T + T_0)w - \partial_j \partial_j T = \frac{Di}{Ra}\Phi + H \tag{4}$$

where adiabatic (de)compression and thermal diffusion correspond to the third and fourth term in the left hand side, respectively. Viscous dissipation and radiogenic heating are included through the first and second right hand terms, respectively.

2.2. Boundary and initial conditions

The subduction process is modeled in a 2-D Cartesian box of 2000 km deep and 2600 km wide. High lower mantle viscosity in this model results in a shallow concentration of the shear,

Table 1
Notations

Parameter	Meaning	Value used	Dimension
A	pre-exponential flow law parameter	–	$Pa^{-n}\ s^{-1}$
ΔA	variation of A relative to values in Table 2	–	–
B	viscosity prefactor = $A^{-1/n}$	–	$Pa\ s^{1/n}$
C	composition parameter	–	–
d	smoothness of the stiffness variation	1000	m
Di	dissipation number = $\alpha g h/c_p$	0.47	–
E^*	activation energy	–	$J\ mol^{-1}$
e	2nd invariant of the strain rate tensor e_{ij}	–	s^{-1}
e_{ij}	$e_{ij} = \partial_j u_i + \partial_i u_j$ = strain rate tensor	–	s^{-1}
H	non-dimensional radiogenic heat production	–	–
n	viscosity stress exponent	–	–
r	subduction to overriding velocity ratio	–	–
R	gas constant	8.3143	$J\ K^{-1}\ m^{-3}$
Ra	Rayleigh number = $\rho\alpha\Delta T h^3/\eta\kappa$	1.8×10^7	–
Rc	compositional Rayleigh number $\Delta\rho_c g h^3/\eta\kappa$	2.4×10^7	–
S	stiffness of the fault = $S_0(1+\tanh(z-z_0)/d)$	–	$Pa\ s\ m^{-1}$
S_0	maximum stiffness of the fault	10^{19}	$Pa\ s\ m^{-1}$
T	non-dimensional temperature	–	–
T_0	non-dimensional surface temperature	$273/\Delta T$	–
Δp	non-dimensional hydrodynamic pressure	–	–
ΔT	temperature contrast across model domain	2300	K
t	non-dimensional time	–	–
$\boldsymbol{u}$	non-dimensional velocity $\boldsymbol{u} = (v,w)^T$	–	–
V^*	activation volume	–	$m^3\ mol^{-1}$
v_0	overriding velocity	–	$cm\ yr^{-1}$
v_{subd}	subduction velocity	–	$cm\ yr^{-1}$
z_0	locking depth in stiffness definition	–	m
η	non-dimensional viscosity	–	–
Φ	non-dimensional viscous dissipation	–	–
ρ_c	crustal density	3116	$kg\ m^{-3}$
ρ_m	mantle density	3416	$kg\ m^{-3}$
τ_{ij}	deviatoric stress tensor	–	Pa
τ	2nd invariant of the stress tensor τ_{ij}	–	Pa

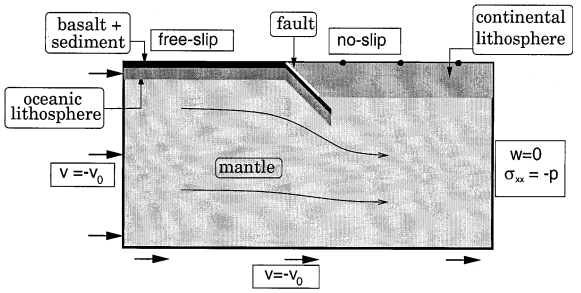

Fig. 1. Description of the mechanical boundary conditions: relative motion between continent and mantle (at left hand vertical and bottom boundary) is imposed. Free slip and fully developed horizontal flow ($\sigma_{xx} = -p$) conditions are used for the oceanic surface and right hand boundary, respectively.

which makes the results relatively insensitive to the depth of the model truncation boundary. Boundary and initial conditions are shown schematically in Fig. 1. Initially the shallow part of the model is divided into an oceanic and a continental lithosphere. The geotherm of the oceanic lithosphere and mantle is based on the cooling of an initially adiabatic temperature distribution with a 1300°C potential temperature. The initial geotherm of the continent is defined as a steady state temperature profile using crustal radiogenic heat production values according to Chapman [28], corresponding to a 60 mW m^{-2} surface heat flow. Oceanic radiogenic heat production is neglected in the models. To avoid the special case of initiation of subduction, we defined an already developed subduction zone: an oceanic plate without a leading slab was thermally and compositionally defined with a 5 cm per year half spreading rate. This plate was subducted with a fixed 5 cm per year subduction velocity for 8 Ma to create the initial condition for further model calculations, with a subducted slab just entering the asthenosphere. We define this moment as time $t = 0$, from which the oceanic surface boundary condition becomes free slip and the convergence rate becomes a free, rather than a fixed parameter. We use this initial condition for all model calculations. The oceanic plate has an age of 8 Ma at the trench. We study the subduction below an actively overriding continent with an ocean-ward velocity $\boldsymbol{v}_0 = (v_0, 0)$ with respect to the deep mantle. Although the reference frame in subduction models is usually fixed to the deep mantle, we choose a 'continental reference frame' here, which is fixed to the top surface of the overriding continental lithosphere, for reasons of computational convenience. To this end, we use a simple galilean coordinate transformation: a no-slip boundary condition is imposed on the continental surface while at the bottom and inflow boundary, a velocity $-\boldsymbol{v}_0$ is imposed, describing again the relative motion between continent and deep mantle. The oceanic surface is modeled as a free slip impermeable boundary, which enables the subduction velocity to develop in a self-consistent way. A horizontal flow and hydrostatic pressure are prescribed on the vertical left hand side boundary. These define the flow to be 'developed', i.e. with a zero horizontal velocity gradient, as in one-dimensional channel flow. Thermal boundary conditions are: 0°C along the top surface $z = 0$, 2300°C at the bottom surface, a continental geotherm at the right hand side boundary and a mantle adiabat at the left hand side boundary $x = 0$, corresponding to an adiabatic gradient of 0.5 K km^{-1} and a potential temperature of 1300°C to represent the mid-ocean ridge.

2.3. Rheological model

The applied mantle rheology is based on a composite rheological model combining both Newtonian and non-Newtonian flow, corresponding to diffusion and dislocation creep respectively [14,27,29,30]. We use an Arrhenius relation for each of the flow components for both mantle and crustal materials:

$$e_{ij} = A\tau^{n-1}\tau_{ij}\exp\left[\frac{E^* + pV^*}{RT}\right] \quad (5)$$

where two sets of values for A, n, E^* and V^* are used for the two creep components. Symbols used are explained in Table 1. Each set of parameters is implemented in the model utilizing the bi-valued composition distribution C. These parameter sets are taken from the literature on experimentally determined flow laws for both upper mantle material and crustal material. Using the second in-

variants e and τ of strain rate and stress, respectively, the definition of the viscosity, $\eta = \tau/e$ and a viscosity prefactor $B = A^{-1/n}$, we define the effective viscosity for each of the two creep components as:

$$\eta = Be^{(1-n)/n}\exp\left[\frac{E^* + pV^*}{RT}\right] \quad (6)$$

and define the effective viscosity as the geometric mean value of the two components [27]. We truncated the effective viscosity at the high end to a value that increases linearly from 10^{20} Pa s to 10^{23} Pa s over the upper 40 km and a constant value of 10^{23} Pa s below this depth. This limits the strength of the cold lithosphere to reasonable values as indicated in, for example, [31]. It essentially substitutes for other, not implemented deformation mechanisms, such as brittle failure or the Peierl's mechanism [32].

Activation parameters E^* and strain rate prefactors A for mantle material are adopted from values given in [29], as listed in Table 2. Comparison of the flow laws for the composite rheology with viscosity estimates from layered post-glacial rebound models [33,34] and geoid inversions [35] suggests a somewhat weaker mantle, although such a comparison is dependent on, for example, chosen geotherm and model dynamics. In order to achieve reasonable viscosity values for the deeper mantle, we define the activation volume for mantle diffusion creep to be 4.5 cm^3 mol^{-1} and for mantle dislocation creep to be 14 cm^3 mol^{-1} [36]. We increased the prefactors A for both diffusion and dislocation creep with respect to [29] with half an order of magnitude to define an appropriate mantle strength for our reference model. This results in a reduction of the viscosity.

The strength of the 7 km thick basaltic oceanic crust is less accurately determined than the strength of olivine, and fewer data are available. Moreover, water plays an important role in the strength determination of crustal materials [31], but amounts of water in subducting oceanic crust are not well known. We use the crustal flow law data from [37], to which we added a roughly estimated activation volume of 10 cm^3 mol^{-1}, and from which we increased the prefactor A from Eq. 5 with two orders of magnitude to define a suitable crustal strength description for the crust in our reference model. Basalt is known to transform into denser and stronger eclogite during subduction. The depth range of this transition in subduction zones is not well known due to poorly known kinetics of the phase transition as a function of interplate contact length, slab temperature and water content [1,12,38–40]. In this model we use a simple approach, in which we assume the crust to have properties intermediate between basalt and eclogite. Taking an intermediate value of -300 kg m^{-3} for the relative crustal density compensates for the absence of a light depleted harzburgitic layer beneath the crust. A more detailed study of the buoyancy effects of the subducting slab and the rheological implications of the basalt-to-eclogite transition is subject of future research.

2.4. Implementation of a lithospheric fault

The dynamics of plate convergence is best described by faulted plate interfaces [14]. To account for the effects of frictional sliding [31] and mylonitic shear localization behavior [41] in the upper part of the subduction zone, we implemented a static fault, with an arc-shaped geometry, as a reasonable approximation of the actual subduction geometry [42]. In general, the fault has to be mobile and advected as in [14,43] in order to adjust to the stress and flow field. The rather rigid

Table 2
Rheology parameters

Rock/mineral	A (Pa^{-n} s^{-1})	n	E^* (J mol^{-1})	Reference
ST: Maryland diabase	8.8×10^{-25}	3.4	260×10^3	[37]
KW: dry diff. olivine	1.92×10^{-11}	1.0	300×10^3	[29]
KW: dry disl. olivine	2.42×10^{-16}	3.5	540×10^3	[29]

overlying continent and relatively short time scales of the presented processes, however, justify the assumption of a rigid fault. The dip angle of the fault increases from zero (horizontal) at the surface to 23° at its deepest part at 100 km depth. Flow across the fault is not allowed and fault friction is defined using a fault stiffness definition, as described in [43]. This way, the slip across a fault plane is coupled to the resisting shear force using $\tau = -Sv$, in which τ is the component of the stress, tangential to the fault and v the slip velocity tangential to the fault. S is the stiffness coefficient, parameterized as a hyperbolic tangent:

$$S = S_0\left(1 + 1/2 \tanh\left(\frac{z - z_0}{d}\right)\right) \quad (7)$$

in which z_0 and d control the depth and smoothness of the fault locking zone. All experiments have $d = 1$ km, which results in a sharply determined locking depth.

3. Numerical techniques

In order to solve Eqs. 1, 2 and 4, we use the finite element package SEPRAN [44]. A penalty function method is used to solve the momentum equation, while the energy equation is integrated in time using a predictor–corrector scheme [27]. A Lagrangian tracer particle method is used to solve Eq. 3. 200 000 tracers are placed in and around the oceanic crustal layer. Each tracer corresponds to a particular parameter value C which is used to define the type of material, crust or mantle at the current tracer position. These tracer values are interpolated to the finite element mesh in the computation of the coefficients of the finite element equations. Tracers are advected with the flow field, using the 4th order Runge–Kutta scheme. Modeling of the relatively small-scale crust requires strong local mesh refinement and the usage of a locally high tracer density.

4. Results

We investigated the efficiency of subduction of an oceanic lithosphere below an overriding lithosphere. Different factors in our numerical model can influence the subduction of the oceanic lithosphere below the overriding plate. Of these, we examined in particular: (1) the depth at which the subduction fault locks, (2) the viscosity of the basaltic crust, (3) the strength of the mantle, (4) viscous dissipation, and (5) the overriding plate velocity. Table 3 lists the complete series of modeling experiments, where model A is used as a reference model. Viscosity prefactors are defined relative to the flow laws from Table 2. Physical parameters are defined in Table 1. Fig. 2 il-

Table 3
Model parameters

Model	A_{mantle}	A_{crust}	z_0 (km)	v_0 (cm yr^{-1})	Φ on/off	v_{subd} (cm yr^{-1})	r	Power (kW m^{-1})
A	$10^{+0.5}$ KW	10^{-2} ST	100	5	on	3.49	0.698	14.0
B	$10^{+0.5}$ KW	10^{-2} ST	100	5	off	2.81	0.562	12.9
C1	$10^{-0.5}$ KW	10^{-2} ST	100	5	on	3.86	0.772	23.8
C2	KW	10^{-2} ST	100	5	on	3.68	0.736	17.4
C3	10^{+1} KW	10^{-2} ST	100	5	on	3.29	0.658	28.7
D1	$10^{+0.5}$ KW	10^{-2} ST	40	5	on	0.84	0.168	9.8
D2	$10^{+0.5}$ KW	10^{-2} ST	60	5	on	1.31	0.262	10.1
D3	$10^{+0.5}$ KW	10^{-2} ST	80	5	on	2.14	0.428	11.9
E1	$10^{+0.5}$ KW	ST	100	5	on	1.88	0.376	11.0
E2	$10^{+0.5}$ KW	10^{-1} ST	100	5	on	2.53	0.506	11.9
E3	$10^{+0.5}$ KW	10^{-3} ST	100	5	on	4.42	0.884	19.8
E4	$10^{+0.5}$ KW	10^{-4} ST	100	5	on	5.33	1.066	17.9
F1	$10^{+0.5}$ KW	10^{-2} ST	100	2.5	on	2.87	1.148	9.2
F2	$10^{+0.5}$ KW	10^{-2} ST	100	7.5	on	3.83	0.510	20.8
F3	$10^{+0.5}$ KW	10^{-2} ST	100	10	on	4.16	0.416	29.1

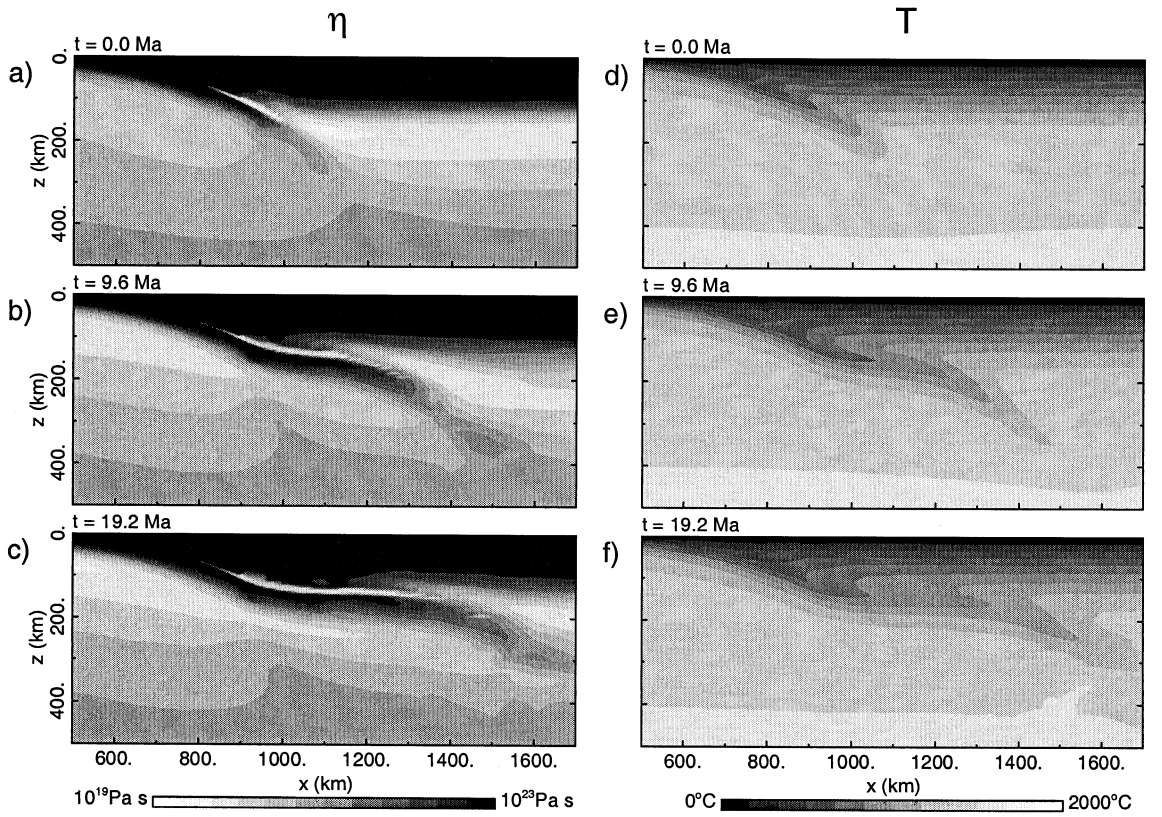

Fig. 2. Viscosity (logarithmic contours) and temperature of reference model A. Three time snapshots at $t=0$ (top panel), 9.6 and 19.2 Ma (bottom panel) since the onset of obduction are shown. The oceanic plate subducts horizontally, creating a doubled lithosphere of increasing horizontal length.

lustrates typical modeling results of the ongoing subduction process for model A. Shown are three snapshots of different times of the effective viscosity (Fig. 2a,b,c) and temperature (Fig. 2d,e,f). The outlines of the subducting slab are revealed by the dark areas, indicating low temperature and high viscosity. In the viscosity plots, the stiff oceanic and continental lithosphere is shown in black. In between, the much weaker oceanic crust is present. In both the viscosity and the temperature plots, an eventually horizontally subducted slab is clearly recognized. The subduction velocity gradually lowers from 5 to 3 cm yr^{-1} within the first 20 Ma due to increasing friction along the increasing plate contact zone. Time averaged values of the different models for the first 20 Ma are presented in Table 3 to quantify the subduction velocity. These subduction velocities are computed as horizontal velocities of the stiff oceanic plate just before subduction.

4.1. The influence of the fault locking depth on subduction

The mechanical coupling on the lithospheric fault is defined by a relation between the local slip velocity along the fault and the local fault shear stress, resisting the slip on the contact plane. The coupling behavior is controlled by the spatially variable stiffness S, as defined in Eq. 7. We set the fault locking depth to 40, 60, 80 or 100 km depth. Table 3 gives the time averaged subduction velocities for each of the experiments, listed as cases D1 to D3 and model A, respectively. In Fig. 3a, the resulting subduction rates are plotted against fault locking depth. At depths larger than

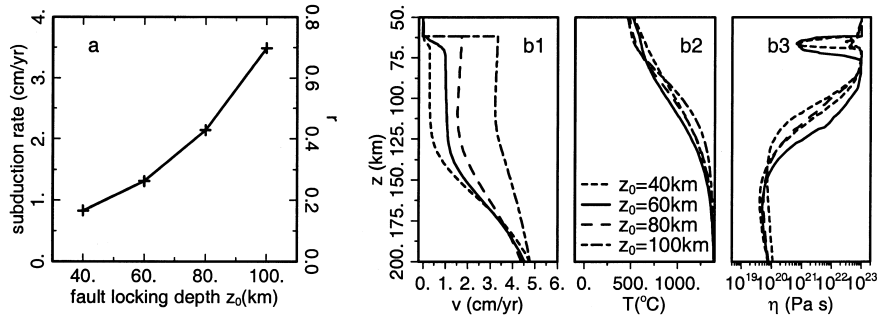

Fig. 3. (a) Subduction rate changes and ratio r are plotted for a variation in the fault locking depth. (b) Vertical profiles at $x = 800$ km (in the middle of the subduction zone) at $t = 9.6$ Ma show the effect of the changing fault depth on (b1) the horizontal velocity component v_x, (b2) the temperature field T, and (b3) the effective viscosity η.

the locking depth, the deformation is taken over by the crustal layer, which is relatively weak and acts as a lubricant. When the unlocked part of the fault is shortened, the length of the crustal shear zone increases. This increases the total resistance against subduction and decreases the subduction velocity. Fig. 3b shows vertical cross sections of several physical quantities at $x = 800$ km (through the subduction zone) and $t = 9.6$ Ma, which clarify the effects of changing the fault depth. Fig. 3b1 shows that for shallow fault locking depths, the velocity increase from continent to slab mainly occurs gradually within the 7 km thick oceanic crust. The models with deeper fault locking depth, however, have the total velocity jump concentrated at the fault above the crust. This fault coupling depth influences the effective viscosity of the crust, as shown in Fig. 3b3.

4.2. The influence of the crustal strength on subduction

In further experiments, the fault coupling depth z_0 is kept constant at 100 km depth. The influence of the intrinsic crustal strength was investigated by varying the prefactor A in Eq. 5, relatively to the value from Table 2. Different model calculations are listed as cases E1–E4 and case A in Table 3. The crustal viscosity is approximately proportional to $\Delta B = \Delta A^{-1/n}$. Fig. 4a and b1 show that the subduction rate strongly depends on the viscosity of the crustal layer. Variation of A of four orders of magnitude, used in this experiment, can be related to the variations in degree of hydration of the subducting oceanic crust. A measure of the effectiveness of obduction is defined through the ratio of the subduction rate and the

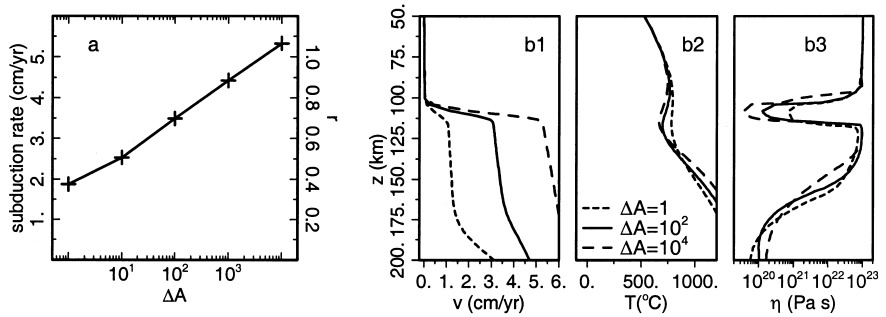

Fig. 4. (a) Subduction rates and velocity ratio r are plotted for different values of the crustal viscosity prefactor ΔA relative to the prefactor from Table 2. (b) Vertical profiles behind the subduction zone ($x = 920$ km) at $t = 9.6$ Ma show the effect of a changing crustal flow law prefactor on (b1) the horizontal velocity component v_x, (b2) the temperature field T, and (b3) the effective viscosity η.

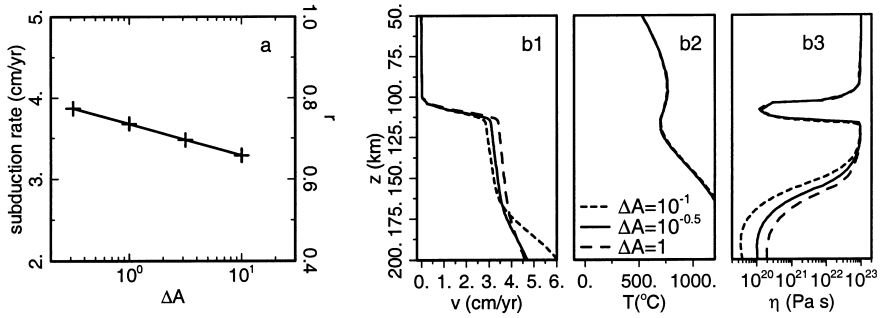

Fig. 5. Similar to Fig. 4 for different values of the mantle viscosity prefactor ΔA, relative to the prefactors for diffusion and dislocation creep from Table 2.

overriding plate velocity $r = v_{subd}/v_0$. Corresponding values of r are given in Figs. 3a and 4a and in Table 3.

4.3. The influence of the mantle rheology on subduction

The mantle rheology is probably not known more accurate than order of magnitude precision. It is therefore worthwhile to examine the influence of variations in the mantle strength on the subduction behavior. We varied the mantle viscosity in cases C1–C3 and case A from Table 3 through changes in the prefactors A of both diffusion and dislocation creep laws in Eq. 5, relatively to the values from Table 2. Resulting subduction rates, temperature profiles and effective viscosity are shown in Fig. 5. Subduction rates increase moderately with increasing mantle strength. For the strongest mantle, the subducting lithosphere couples best to the mantle below since the asthenosphere is then least pronounced. This prevents the subducting plate from colliding and being pushed along with the overriding plate and therefore results in the highest subduction rates. The drag of the oceanic plate with the mantle below in these models is therefore necessary for subduction to occur. This is opposite to the situation in Benioff subduction, in which the mantle drag usually is thought to resist the subduction process. For the reference model A, the ratio of diffusion creep viscosity over dislocation creep viscosity is shown in Fig. 6. The high values of the ratio in the strong lithosphere and surrounding (including the asthenosphere) are indicative of local predominance of dislocation creep flow over the diffusion creep component. This indicates that the change in dislocation creep strength is most important here. Diffusion creep governs the mantle strength at greater depths, which is in line with [29]. Another feature, that is at least partly controlled by mantle strength, is the ability of the overriding plate to avoid the slab from subducting further to the deep mantle (Benioff type of subduction). The mantle will be able to support the (small) weight of the young slab only when it has enough strength to resist the necessary deformation involved. If not, the slab will subduct further, once asthenospheric material is able to penetrate in between the two lithospheres. Such an event occurred in model C3 with a relatively weak mantle and is shown in Fig. 7. Non-linear rheology, in combination with viscous heating weakened the slab during bending and caused slab detachment.

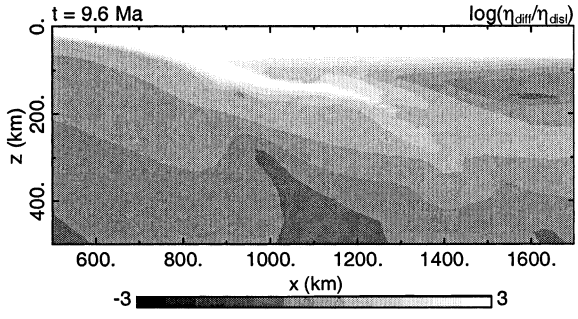

Fig. 6. The logarithmic ratio of diffusion creep viscosity over dislocation creep viscosity for the reference model A at $t = 9.6$ Ma indicates that dislocation creep is the main deformation mechanism in and near the lithospheres, while at deeper levels, diffusion creep becomes dominant.

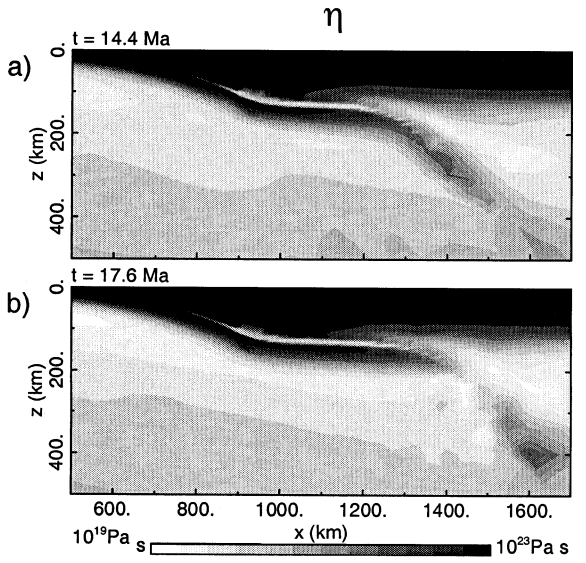

Fig. 7. Viscosity plot for model C3 for time $t = 14.4$ and $t = 17.6$ Ma, in which the subduction of the slab through a relatively weak mantle is shown. Non-linear rheology and viscous heating lead to the detachment of slab in the bending area.

4.4. The role of viscous heating in the subduction process

We compared the results from two models, listed as cases A and B in Table 3, for calculations with and without viscous heating, respectively. The time averaged subduction velocity is 2.81 cm yr^{-1} for model B and increases to 3.49 cm yr^{-1} for model A. Fig. 8 shows vertical cross sections of the relevant physical quantities for both models A and B, again at $x = 920$ km for $t = 9.6$ Ma. Viscous dissipation heats the crustal layer, as shown in Fig. 8b, where most of the shear deformation occurs. This results in a decrease of effective crustal viscosity of half an order of magnitude, as shown in Fig. 8c, due to both the temperature and the strain rate dependence of the viscosity. These effects enhance mechanical decoupling resulting in an increase of the subduction rate.

4.5. Relation between subduction velocity and overriding plate velocity

In the previous experiments, a constant velocity

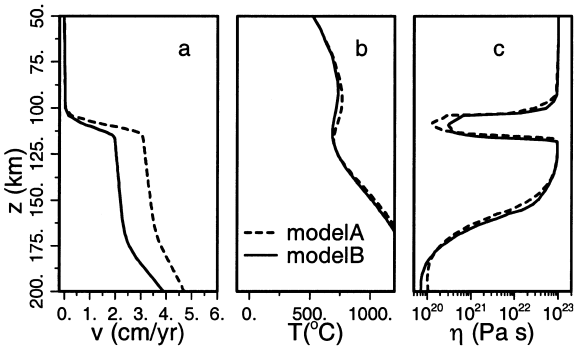

Fig. 8. Vertical profiles at $x = 920$ km for $t = 9.6$ Ma for a model with viscous dissipation (A) and without (B). Shown are horizontal velocity, temperature and effective viscosity.

of the overriding plate $v_0 = 5$ cm yr^{-1} was used. In models F1–F3 (Table 3), we varied the overriding velocity between 2.5 and 10 cm yr^{-1} to examine its effect on the subduction behavior. Fig. 9 indicates a convergence rate increasing with increasing overriding plate velocity. This relation is non-linear: an increasing overriding velocity leads to a larger shear, which in turn results in lower dislocation creep strength and more shear heating. This causes a more pronounced asthenosphere with less coupling between the mantle and subducting plate and a less effective obduction, as indicated through the lower velocity ratio r in Table 3.

5. Discussion

In our model, the overriding plate provides a

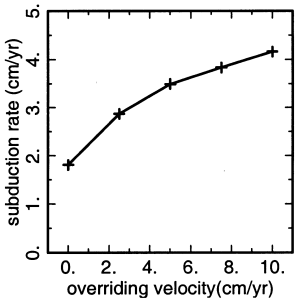

Fig. 9. The relation between the overriding and subduction velocities. The relation is non-linear, due to the non-linear dislocation creep strength: a larger strain rate leads to a lower viscosity in the asthenosphere.

driving mechanism for young oceanic plates to subduct, thereby constantly performing work on the system. In our model, the corresponding work per unit time, or power, is introduced through the velocity boundary conditions that describe the relative motion between continent and deep mantle. Validation of the model by an estimate of this additional work is necessary [45]. We make an estimate of this power input by assuming that the dissipated energy of the model is provided mainly by the imposed boundary conditions (external energy source), since the potential energy release is small for a young oceanic plate that subducts only to a depth of about 120 km, as is the case in our models. The time averaged generated power of viscous heating of the reference model is 14.1×10^3 W m^{-1}. In case Benioff subduction occurs (as in model C3, Table 3), this value becomes larger, because in that case the release of potential energy by the sinking slab becomes significant. In case of a stronger mantle (models C1 and C2, Table 3), this value increases as well: the asthenosphere is less pronounced and the involved overriding shear stress increases. This suggests that the estimated work done by the overriding continent per unit time puts a constraint on the mantle strength in this model. If we assume the overriding continent to be driven by forces of the same order of magnitude as ridge push ($\approx2\times10^{12}$ N m^{-1}), a corresponding estimate of the amount of work per unit of time done by a 5 cm per year overriding continent on the system is $3\text{–}4\times10^3$ W m^{-1}. These values, however, may be larger when besides young subduction also older slabs subduct at the same subduction zone in a 3-D configuration, in which case the pulling force of slab roll-back may contribute considerably. This may for example be the case at the west coast of South America [13]. These estimates show that the power, introduced by the velocity boundary conditions, is probably of the correct order of magnitude.

Although here the emphasis is put on the significance of the rheology for shallow flat subduction, another important model parameter is the buoyancy of the slab. A heavy slab will be able to subduct steeply more easily than a buoyant one. The buoyancy of the slab is influenced by the age of the slab, the stratigraphy of the oceanic plate and the series of phase transitions from basalt to eclogite [39]. These aspects of the subduction process are subject of further research.

6. Concluding remarks

We have performed numerical model experiments for a passive oceanic lithosphere that is overridden by a continent. We varied the physical parameters that influence the friction between the two converging plates. This influence is clearly expressed in the ratio of the subduction velocity over the overriding plate velocity. We modeled a subduction fault that partly decouples the plates, as well as a crustal layer with a rheology that is significantly weaker than the mantle rheology. Both the crustal strength and locking depth of the fault influence the subduction rate significantly. The mantle strength must be large enough to fix the overridden oceanic plate to the underlying mantle and to prevent steep Benioff type subduction to develop. However, the mantle cannot be too viscous in view of the limited driving force of the overriding plate. In the model calculations, viscous heating turned out to be an significant factor facilitating subduction. Non-linear dislocation creep included in our composite rheological model appears to be important in weakening the shallow subducting crust and mantle, whereas in the deeper parts linear diffusion creep is dominant, in line with predictions of [29]. The ratio of subduction and overriding velocity was shown to depend non-linearly on the overriding velocity due to the presence of mantle power law creep. In conclusion: from numerical experiments, we have found active obduction of oceanic lithosphere by an overriding continent to be a viable mechanism for shallow flat subduction over a wide range of parameters.

Acknowledgements

The authors would like to thank M. Gurnis and M. Riedel for highly constructive reviews which helped to improve the manuscript substantially.

We thank David Yuen for the helpful discussions and Guus Segal for the help in applying the SEPRAN finite element package. We acknowledge NATO for financial support. Work was done in part, while J.v.H. and A.v.d.B. were visiting the Minnesota Supercomputing Institute.*[RV]*

References

[1] N.J. Vlaar, Thermal anomalies and magmatism due to lithospheric doubling and shifting, Earth Planet. Sci. Lett. 65 (1983) 322.
[2] D.C. Engebretson, A. Cox, R.G. Gordon, Relative motions between oceanic and continental plates in the pacific basin, special paper, No. 286, Geological Society of America, 1985, pp. 1–59.
[3] R.G. Gordon, D.M. Jurdy, Cenozoic global plate motions, J. Geophys. Res. 91 (B12) (1986) 12389–12406.
[4] A.E. Gripp, R.G. Gordon, Current plate velocities relative to the hotspot incorporating the Nuvel-1 global plate motion model, Geophys. Res. Let. 17 (1990) 1109–1112.
[5] C. Doglioni, The global tectonic pattern, J. Geodyn. 12 (1990) 21–38.
[6] N.J. Vlaar, M.J.R. Wortel, Lithospheric aging, instability and subduction, Tectonophysics 32 (1976) 331.
[7] T.A. Cross, R.H. Pilger Jr., Controls of subduction geometry, location of magmatic arcs, and tectonics of arc and back-arc regions, GSAB 93 (1982) 545–562.
[8] P. Bird, Formation of the rocky mountains, Western United States: A continuum computer model, Science 239 (1988) 1501–1507.
[9] J.E. Spencer, Uplift of the Colorado Plateau due to lithosphere attenuation during Laramide low-angle subduction, J. Geophys. Res. 101 (B6) (1996) 13595–13609.
[10] S. van der Lee, G. Nolet, Seismic image of the subducted trailing fragments of the Farallon plate, Nature 386 (1997) 266–269.
[11] M.J.R. Wortel, N.J. Vlaar, Age-dependent subduction of oceanic lithosphere beneath western South America, Phys. Earth Planet. Inter. 17 (1978) 201–208.
[12] I.S. Sacks, The subduction of young lithosphere, J. Geophys. Res. 88 (B4) (1983) 3355–3366.
[13] M.-A. Gutscher, J. Malavieille, S. Lallemand, J.-Y. Collot, Tectonic segmentation of the North Andean margin: impact of the Carnegie ridge collision, Earth Planet. Sci. Lett. 168 (1999) 255–270.
[14] S. Zhong, M. Gurnis, Mantle convection with plates and mobile, faulted plate margins, Science 267 (1995) 838–843.
[15] U.R. Christensen, The influence of trench migration on slab penetration into the lower mantle, Earth Planet. Sci. Lett. 140 (1996) 27–39.
[16] D. Olbertz, The long-term evolution of subduction zones: a modelling study, Ph.D. thesis, Utrecht University, Utrecht, 1997.
[17] M.C. Jischke, On the dynamics of descending lithospheric plates and slip zones, J. Geophys. Res. 80 (1975) 4809–4813.
[18] D.J. Stevenson, S.J. Turner, Angle of subduction, Nature 270 (1977) 334–336.
[19] A. Tovish, S. Schubert, B.P. Luyendyk, Mantle flow pressure and the angle of subduction: non-newtonian corner flows, J. Geophys. Res. 83 (B12) (1978) 5892–5898.
[20] S. Zhong, M. Gurnis, L. Moresi, Role of faults, nonlinear rheology, and viscosity structure in generating plates from instantaneous mantle flow models, J. Geophys. Res. 103 (B8) (1998) 15255–15268.
[21] A.P. van den Berg, D.A. Yuen, P.E. van Keken, Effects of depth-variations in creep laws on the formation of plates in mantle dynamics, Geophys. Res. Lett. 18 (1991) 2197–2200.
[22] R. Trompert, U. Hansen, Mantle convection simulations with rheologies that generate plate-like behaviour, Nature 395 (1998) 686–689.
[23] A. Lenardic, W.M. Kaula, Self-lubricated mantle convection: two-dimensional models, Geophys. Res. Lett. 21 (1994) 1707–1710.
[24] D.A. Yuen, L. Fleitout, G. Schubert, Shear deformation zones along major transform faults and subducting slabs, Geophys. J. R. Astron. Soc. 54 (1978) 93–119.
[25] B. Schott, D.A. Yuen, H. Schmeling, Viscous heating in heterogeneous media as applied to the thermal interaction between crust and mantle, Geophys. Res. Lett. 26 (1999) 513–516.
[26] J. Ita, S.D. King, Sensitivity of convection with an endothermic phase change to the form of governing equations, initial conditions, boundary conditions, and equation of state, J. Geophys. Res. 99 (B8) (1994) 15919–15938.
[27] A.P. van den Berg, P.E. van Keken, D.A. Yuen, The effects of a composite non-Newtonian and Newtonian rheology on mantle convection, Geophys. J. Int. 115 (1993) 62–78.
[28] D.S. Chapman, Thermal gradients in the continental crust, in: J.B. Dawson, D.A. Carswell, J. Hall, K.H. Wedepohl (Eds.), The Nature of the Lower Continental Crust, Geological Society, 1986, pp. 63–70.
[29] S. Karato, P. Wu, Rheology of the upper mantle: a synthesis, Science 260 (1993) 771–778.
[30] A.P. van den Berg, D.A. Yuen, Modelling planetary dynamics by using the temperature at the core-mantle boundary as a control variable: effects of rheological layering on mantle heat transport, Phys. Earth Planet. Inter. 108 (1998) 219–234.
[31] D.L. Kohlstedt, B. Evans, S.J. Mackwell, Strength of the lithosphere: Constraints imposed by laboratory experiments, J. Geophys. Res. 100 (B9) (1995) 17587–17602.
[32] M. Kameyama, D.A. Yuen, S.-I. Karato, Thermal-mechanical effects of low-temperature plasticity (the Peirels mechanism) on the deformation of a viscoelastic shear zone, Earth Planet. Sci. Lett. 168 (1999) 159–172.
[33] K. Lambeck, P. Johnston, The viscosity of the mantle: Evidence from analysis of glacial-rebound phenomena, in:

The Earth's Mantle: Composition, Structure and Evolution, Cambridge University Press, Cambridge, 1998, Ch. 10, pp. 461–502.
[34] K. Lambeck, C. Smither, P. Johnston, Sea-level change, glacial rebound and mantle viscosity for northern Europe, Geophys. J. Int. 134 (1998) 102–144.
[35] B.H. Hager, Mantle viscosity: a comparison of models from postglacial rebound and from the geoid, plate driving forces, and advected heat flux, in: R. Sabadini (Ed.), Glacial Isostasy, Sea-level and Mantle Rheology, Kluwer Academic Publishers, Dordrecht, 1991, pp. 493–513.
[36] S. Karato, D.C. Rubie, Toward an experimental study of deep mantle rheology: A new multianvil sample assembly for deformation studies under high pressures and temperatures, J. Geophys. Res. 102 (B9) (1997) 20111–20122.
[37] G. Shelton, J. Tullis, Experimental flow laws for crustal rocks, EOS 62 (1981) 396.
[38] T.J. Ahrens, G. Schubert, Gabbro-eclogite reaction rate and its geophysical significance, Rev. Geophys. Space Phys. 13 (1975) 383–400.
[39] B.R. Hacker, Eclogite formation and the rheology, buoyancy, seismicity and H_2O content of oceanic crust, in: Subduction: Top to Bottom, AGU Geophysical Monograph, 1996, pp. 337–346.
[40] I. Iwamori, Transportation of H_2O and melting in subduction zones, Earth Planet. Sci. Lett. 160 (1998) 65–80.
[41] D. Jin, S.-I. Karato, M. Obata, Mechanisms of shear localization in the continental lithosphere: inferences from the deformation microstructures of peridotites from the Ivrea zone, northwestern Italy, J. Struct. Geol. 20 (1998) 195–209.
[42] J. van den Beukel, R. Wortel, Thermo-mechanical modeling of arc-trench regions, Tectonophysics 154 (1988) 177–193.
[43] J. Toth, M. Gurnis, Dynamics of subduction initiation at preexisting fault zones, J. Geophys. Res. 103 (B8) (1998) 18053–18067.
[44] G. Segal, N.P. Praagman, SEPRAN user's guide, Tech. rep., SEPRA, Technical University Delft, 1995.
[45] L. Han, M. Gurnis, How valid are dynamic models of subduction and convection when plate motions are prescribed?, Phys. Earth Planet. Inter. 110 (1999) 235–246.